AIP | Journal of Applied Physics

Visible to near infrared conversion in Ce3+–Yb3+ Co-doped YAG ceramics

Jumpei Ueda and Setsuhisa Tanabe

Citation: J. Appl. Phys. **106**, 043101 (2009); doi: 10.1063/1.3194310
View online: http://dx.doi.org/10.1063/1.3194310
View Table of Contents: http://jap.aip.org/resource/1/JAPIAU/v106/i4
Published by the American Institute of Physics.

Visible to near infrared conversion in $Ce^{3+}-Yb^{3+}$ Co-doped YAG ceramics

Jumpei Ueda[a] and Setsuhisa Tanabe
Graduate School of Human and Environmental Studies, Kyoto University, Yoshida-nihonmatsu-cho Sakyo-ku, Kyoto 606-8501, Japan

(Received 25 June 2009; accepted 7 July 2009; published online 17 August 2009)

In $Ce^{3+}-Yb^{3+}$ co-doped $Y_3Al_5O_{12}$ (YAG) ceramics, possibility of quantum cutting mechanism converting one visible photon into two NIR photons with optimum quantum efficiency approaching 200% have been investigated. In this material, Yb^{3+} emissions due to the $^2F_{5/2}$-$^2F_{7/2}$ in the range of 1 μm were observed upon the excitation of 5*d* level of Ce^{3+}. In addition, excitation spectra of Yb^{3+} emission corresponded to that of Ce^{3+} emission completely. Lifetime of the 5*d* level of Ce^{3+} decreased with increasing Yb^{3+} content. These results indicate the energy transfer (ET) from the 5*d* levels of Ce^{3+} to the $^5F_{5/2}$ level of Yb^{3+}. In $(Y_{0.945}Ce_{0.005}Yb_{0.05})_3Al_5O_{12}$ sample, the directly measured quantum yield (QY) of Yb^{3+} emission upon the excitation of 5*d* level of Ce^{3+} was about 12% and lower than QY (96%) that estimated from the ET efficiency which was calculated with the measured lifetime of Ce^{3+}. © *2009 American Institute of Physics*. [DOI: 10.1063/1.3194310]

I. INTRODUCTION

Luminescent materials doped with rare earth ions are used for many devices such as optical amplifiers in telecommunication, phosphors for white light emitting diodes (LEDs), displays, and so on. Recently, they also have attracted a great interest for photovoltaic applications to improve solar cell efficiency by modifying solar spectrum.[1] Figure 1 shows the solar spectrum and the spectral response of crystalline silicon solar cell. Crystal silicon (*c*-Si) solar cells most effectively convert photons of energy close to the semiconductor band gap. The mismatch between the incident solar spectrum and the spectral response of solar cells is one of the main reasons to limit the cell efficiency. The efficiency limit of the *c*-Si have been estimated to be 29% by Shockley and Queisser.[2] However, this limit is estimated to be improved up to 38.4% by modifying the solar spectrum by a quantum cutting (downconverting) phosphor which converts one photon of high energy into two photons of lower energy.[3]

The phenomenon such as the quantum cutting or the downconversion of rare earth ions have been investigated since Dexter[4] reported the possibility of a luminescent quantum yield greater than unity in 1957. In the past, the quantum cutting from a vacuum ultraviolet photon to visible photons for Pr^{3+},[5,6] Gd^{3+},[7] $Gd^{3+}-Eu^{3+}$,[8] and $Er^{3+}-Tb^{3+}$[9] had been studied. Recently, a new quantum cutting phenomenon from visible photon shorter than 500 nm to two infrared photons for $Tb^{3+}-Yb^{3+}$,[10–13] $Pr^{3+}-Yb^{3+}$,[14] and $Tm^{3+}-Yb^{3+}$[15] has been reported. The Yb^{3+} ion is suitable as an acceptor and emitter because luminescent quantum efficiency of Yb^{3+} is close to 100% and the energy of the only excited level of Yb^{3+} (~1.2 eV) is roughly in accordance with the band gap of Si (~1.1 eV). However, absorption transitions of Pr^{3+}, Tb^{3+}, and Tm^{3+} as a donor are due to forbidden *f*-*f* transitions. Therefore, the absorption linewidth and cross sections are not so wide and large, respectively. On the other hand, optical transitions of Ce^{3+} in the UV to visible regions are due to allowed *f*-*d* transitions. As a result the absorption linewidth and cross sections are wide and large, respectively. In addition, the Ce^{3+}-doped $Y_3Al_5O_{12}$ (YAG), used as a phosphor for white LED, has broad absorption bands in the range of 300–500 nm due to strong ligand field and high luminescent quantum efficiency.[16,17] Therefore, the Ce^{3+} ions in the YAG can be suitable as an excellent sensitizing donor for down conversion materials of Si solar cells.

In this study, $Ce^{3+}-Yb^{3+}$-codoped YAG ceramics were prepared and the energy transfer (ET) including down conversion mechanism in $Ce^{3+}-Yb^{3+}$ codoped YAG ceramics have been evaluated by the photoluminescence (PL), the photoluminescence excitation (PLE), the lifetime and the quantum yield (QY), which was measured directly using an integrating sphere.

II. EXPERIMENT

Polycrystalline YAG ceramics with composition of $(Y_{0.995-x}Ce_{0.005}Yb_x)_3Al_5O_{12}$ (x=0, 0.005, 0.02, 0.05, and

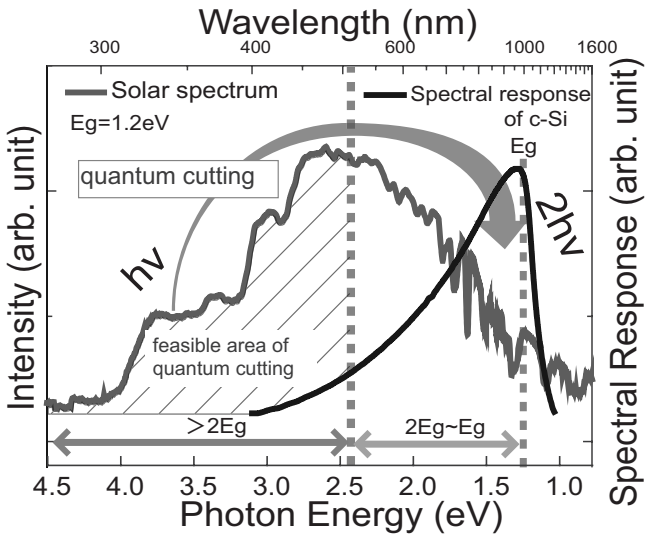

FIG. 1. Solar spectrum and spectral response of *c*-Si.

[a]Electronic mail: j.ueda@at3.ecs.kyoto-u.ac.jp.

0.1) were prepared by using reagent grade Y_2O_3 (99.99%), Al_2O_3 (99.99%), CeO_2 (99.99%), and Yb_2O_3 (99.99%) as starting materials. The powders were mixed well with tetraethyl orthosilicate (0.5 wt %) in an alumina mortar to facilitate solid state reaction, pressed into a pellet of 20 mm diameter and sintered at 1600 °C for 6 h. The first obtained polycrystalline pellets were crushed, pressed and sintered again to obtain complete single phase of YAG. The crystal phases of obtained samples were identified by an x-ray diffraction (XRD) measurement (Shimadzu, XRD6000). For the PL spectra, samples were excited by using 450 nm light that was obtained by combining a band pass filter and a Xe lamp (Asahi Spectra Co., Ltd., MAX-302). The luminescence spectra were measured with a monochromator (Nikon, G250) and a Si photodiode (Electro-Optical System Inc., S-025-H). The obtained PL spectra were calibrated by a standard halogen lamp (Labsphere, OGL-600). In the PLE spectra measurement monitoring near infrared luminescence, the luminescence was detected by combining an 850 nm short cut filter and an InGaAs (Electro-Optical System Inc., IGA-010-H) photodiode. Samples were excited by monochromatic light obtained by combining the Xe lamp (350–800 nm) and the monochromator. For the PLE spectra monitoring visible luminescence, a 550 nm bandpass filter and the Si photodiode were used. For the luminescent decay measurement, samples were excited by using a 466 nm dye (Exciton, LD466) laser pumped with a nitrogen laser pulse excitation. The decay curves of fluorescence at 550 and 1030 nm were detected by a high-speed silicon detector (Thorlabs, Inc., DET110) and averaged on a digital oscilloscope (Yokogawa, DL1620). For the QY of emission upon the excitation of Ce^{3+}:5*d* level, the PL spectra were measured under the 440 nm LD excitation (Nichica, NDHB510APA) by using an integrating sphere (Labsphere) which was connected to a charge coupled device (CCD) detector of visible range (Ocean Optics, USB2000) and a CCD detector of infrared range (Ocean Optics, USB2000+) with an optical bifurcated fiber of 400 μm core. The obtained PL spectra were calibrated by using the standard halogen lamp and an auxiliary lamp (Labsphere, AUX-30), and then the total radiant flux and photon distribution were obtained. The QY was evaluated as the ratio of the emission photon number to the absorption photon number. For the QY of emission upon the excitation of Yb^{3+}, the 935 nm laser diode (LD) (Qphotonics, QLD-945-100S) was used as excitation.

III. RESULTS

A. YAG samples

The XRD patterns of obtained samples are shown in Fig. 2. The XRD patterns of all samples almost corresponded to that of the YAG.[18] The XRD peaks were slightly shifted to higher angle (2θ) with increasing Yb^{3+} content (inset in Fig. 2).

B. Optical property of Ce^{3+} and Yb^{3+} in YAG

1. Photoluminescence and photoluminescence excitation

Figure 3 shows the PL spectrum by 450 nm excitation and the PLE spectra monitoring 550 and 1030 nm of the sample with $x=0.05$ composition. The emission bands peaked at 550 nm (Ce^{3+}:5*d*-4*f*) and 1030 nm (Yb^{3+}:$^2F_{5/2}$-$^2F_{7/2}$) were observed by exciting the 5*d* level of Ce^{3+} with 450 nm light. For the PLE spectrum monitoring 550 nm, the broad excitation bands were located at 330 and 450 nm. For the PLE spectrum monitoring 1030 nm, a broad excitation band located at 450 nm was also observed. These two PLE spectra were consistent between 400 and 500 nm.

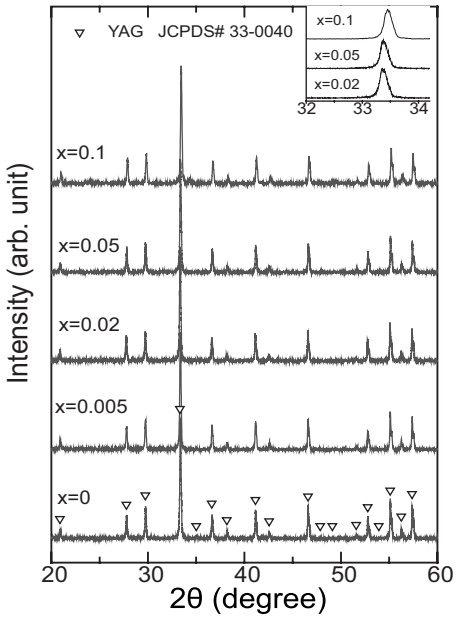

FIG. 2. XRD patterns of Ce^{3+}–Yb^{3+} codoped YAG with different Yb^{3+} contents. (Inset is extend figure of main peak in some samples).

2. Decay curves

Figure 4 shows the decay curves of Ce^{3+} emission at 540 nm under the 466 nm dye laser. Each decay curve was fitted by the following single exponential function:

$$I = I_0 \exp(-t/\tau_{\text{decay}}). \quad (1)$$

It can be seen that the decay times were decreased with increasing Yb^{3+} content. Figure 5 shows the decay curves of emission at 1030 nm due to Yb^{3+} transition ($^2F_{5/2} \rightarrow {}^2F_{7/2}$). In this measurement, both rise and decay components were observed. Each decay curve was fitted by the following double exponential function:

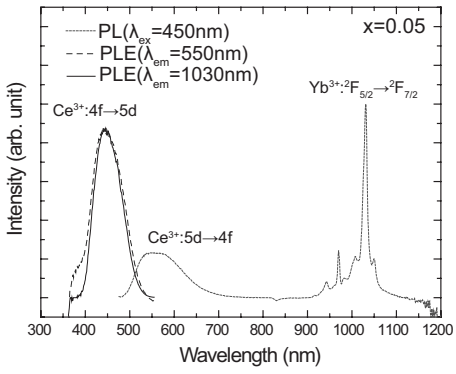

FIG. 3. PL spectrum by the 450 nm LD excitation and PLE spectra monitored at 550 and 1030 nm in Ce^{3+}–Yb^{3+} codoped YAG.

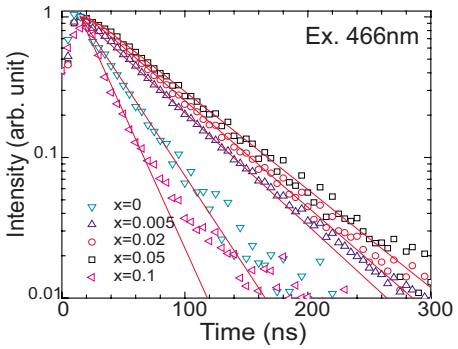

FIG. 4. (Color online) Single logarithmic chart of decay curves, which monitored emission from $5d$ level of Ce^{3+} by 466 nm excitation, in samples with different Yb^{3+} contents.

$$I = I_0\{\exp(-t/\tau_{\text{decay}}) - \exp(-t/\tau_{\text{rise}})\}. \quad (2)$$

IV. TOTAL RADIANT FLUX

Figure 6 shows the total radiant flux spectra of some samples by 440 nm LD excitation. In the sample with $x=0$ composition, the intense emission at around 540 nm was observed, while no emission at around 1030 nm was observed. The intensity of emission at around 540 nm was decreased with increasing Yb^{3+} content, while that at around 1030 nm was increased with increasing Yb^{3+} content until $x=5$ composition. Figure 7 shows the radiant flux spectra of samples in the range of near infrared by 935 nm LD excitation.

V. DISCUSSIONS

A. YAG samples

From the obtained XRD peaks, the lattice constant, a, of the YAG ceramics was estimated by the following equation that combined the Bragg's equation with a relation of cubic lattice constant with the Miller's indices:

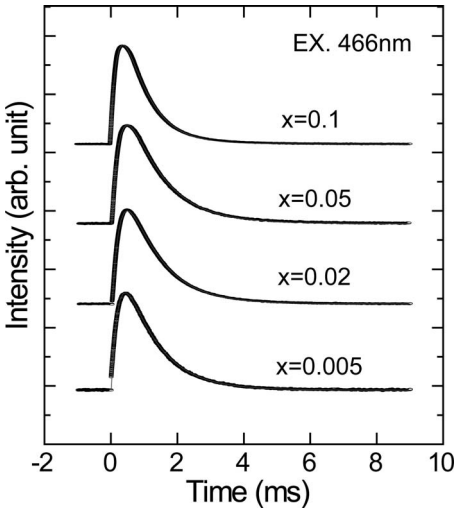

FIG. 5. Yb^{3+} content variation of decay curve, which monitored emission from the $^2F_{5/2}$ of Yb^{3+} by 466 nm excitation.

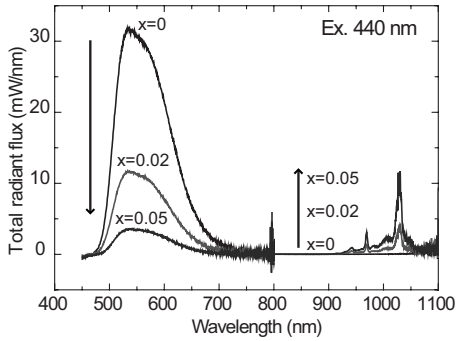

FIG. 6. Yb^{3+} content variation total radiant flux spectra by 440 nm excitation.

$$a = \frac{\lambda\sqrt{h^2+k^2+l^2}}{2\sin\theta}, \quad (3)$$

where λ is the wavelength of Cu K_α radiation, (h,k,l) is the Miller's indices and θ is the angle of diffraction peak. Figure 8 shows the calculated lattice constant and reference crystal of $Y_3Al_5O_{12}$:YAG[18] and $Yb_3Al_5O_{12}$:YBAG.[19] The lattice constant of obtained YAG were decreased with increasing Yb^{3+} content following Vegard's law. Therefore, it was confirmed that Yb^{3+} ions were incorporated into YAG crystal.

B. Optical property of Ce^{3+} and Yb^{3+} in YAG

1. Energy transfer from Ce^{3+} to Yb^{3+}

Results of the PL and PLE spectra of the sample with $x=0.05$ composition in Fig. 3 indicated evidence of energy transfer from the $5d$ levels of Ce^{3+} to the $^2F_{5/2}$ level of Yb^{3+}. The excitation bands of Ce^{3+} correspond to the peak energy of solar spectrum, which is in a range of low spectral response of c-Si. In addition, the emission band peaked at 1030 nm corresponds to a range of high spectral response. Therefore, the ET from Ce^{3+} to Yb^{3+} in YAG ceramics is suitable for solar spectrum convertor from viewpoint spectral characteristics of the PL and the PLE. From decreasing of lifetime of Ce^{3+}:$5d$ level with increasing Yb^{3+} content, it is considered that energy transfer from Ce^{3+} to Yb^{3+} occurred. The total decay rate (W_{tot}) of $5d$ levels in Ce^{3+} single doped YAG sample is given by

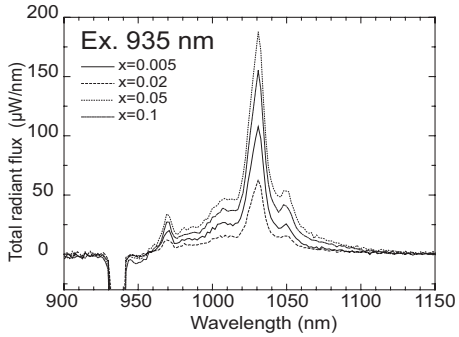

FIG. 7. Yb^{3+} content variation total radiant flux spectra by 935 nm excitation.

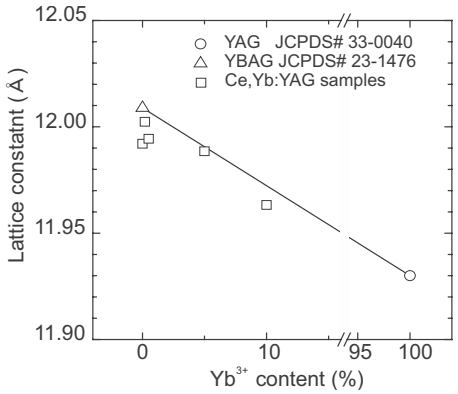

FIG. 8. Yb^{3+} content dependence of lattice constant of $Ce^{3+}-Yb^{3+}$ codoped YAG. Solid line is lattice constant estimated from Vegard's law.

$$W_{\mathrm{tot}} = A + W_{\mathrm{MP}} = \tau_{\mathrm{Ce}}^{-1}, \tag{4}$$

where A is the radiative rate, W_{MP} is the multiphonon relaxation rate, and τ_{Ce} is the lifetime of $5d$ level in Ce^{3+} single doped YAG. In Ce^{3+}, Yb^{3+}-codoped YAG, the extra decay pathway from $5d$ level of Ce^{3+} to $^2F_{5/2}$ level of Yb^{3+} was generated. Therefore, the total decay rate is given by

$$W_{\mathrm{tot}} = A + W_{\mathrm{MP}} + W_{\mathrm{ET}} = \tau_{\mathrm{Ce,Yb}}^{-1}, \tag{5}$$

where W_{ET} is the energy transfer rate and $\tau_{\mathrm{Ce,Yb}}$ is the lifetime of $5d$ level in $Ce^{3+}-Yb^{3+}$ codoped YAG. Therefore the energy transfer efficiency is given by

$$\eta_{\mathrm{ET}} = \frac{W_{\mathrm{ET}}}{A + W_{\mathrm{MP}} + W_{\mathrm{ET}}} = 1 - \frac{\tau_{\mathrm{Ce,Yb}}}{\tau_{\mathrm{Ce}}}. \tag{6}$$

Figure 9 shows the Yb^{3+} content dependences of lifetime for the $5d$ level of Ce^{3+} and the ET efficiency from the $5d$ level of Ce^{3+} to the $^2F_{5/2}$ of Yb^{3+}. The lifetime decreased with increasing Yb^{3+} content, the ET efficiency increased with increasing Yb^{3+} content. The ET efficiency exceeded about 50% above $x=0.05$ composition. Therefore, the quantum yield of Yb^{3+} will be over 100% if ideal quantum cutting occurred as the equation given by

$$\mathrm{QY} = 2\,\eta_{\mathrm{Yb}}\,\eta_{\mathrm{ET}}, \tag{7}$$

where η_{Yb} is the emission quantum efficiency of Yb^{3+}, usually about 100% because of low multiphonon relaxation rate due to large energy gap to the next lower level, the ground

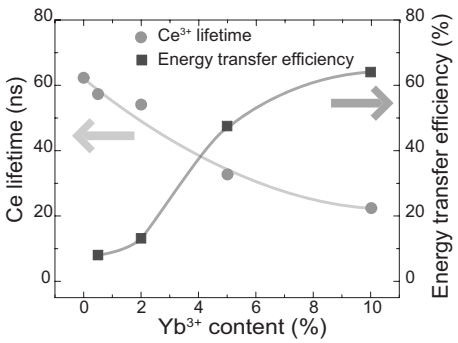

FIG. 9. Yb^{3+} content dependence of lifetime at $5d$ level of Ce^{3+} and energy transfer efficiency from Ce^{3+} to Yb^{3+}.

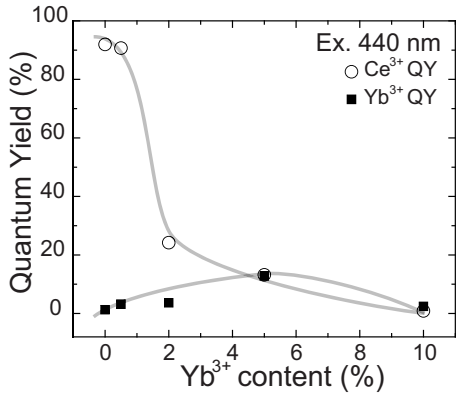

FIG. 10. Yb^{3+} content dependence of quantum yield of Ce^{3+} emission and Yb^{3+} emission by 440 nm excitation.

state. In the sample with $x=0.05$ composition, the QY was estimated high value (96%).

VI. TOTAL RADIANT FLUX

From the total radiant flux spectrum by 440 nm LD excitation, the photon distribution spectrum can be obtained. Therefore the emission and absorption photon number was estimated, and then the quantum efficiency was calculated. Figure 10 shows the Yb^{3+} content dependences of the QY of Ce^{3+} emission at around 550 nm and that of Yb^{3+} emission at around 1030 nm. The QY of Ce^{3+} emission decreased and that of Yb^{3+} emission increased with increasing Yb^{3+} content. The maximum value of QY of Yb^{3+} was 12.8% in the $x=0.05$ sample and lower than that estimated from the ET efficiency, which was calculated with the measured lifetime of Ce^{3+}:$5d$ level. It is considered that other nonradiative processes existed. From the radiant flux spectrum by 935 nm LD excitation, the QY of Yb^{3+} was calculated. Figure 11 shows the Yb^{3+} content dependence of QY of the Yb^{3+} emission by 935 nm LD excitation. At least the QY indicated higher value than 80% until $x=0.05$. Therefore it is considered that the nonradiative processes are not due to concentration quenching of Yb^{3+}.

VII. ENERGY TRANSFER MECHANISM

Figure 12 shows the Yb^{3+} content dependence of rise and decay time of the Yb^{3+} emission by 466 nm excitation.

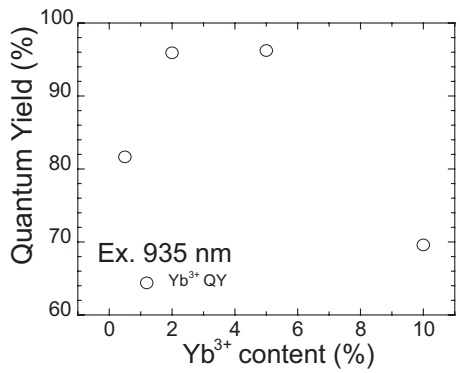

FIG. 11. Yb^{3+} content dependence of quantum yield of Yb^{3+} emission and by 935 nm excitation.

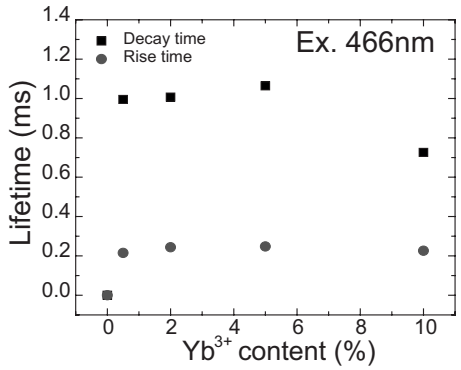

FIG. 12. Yb^{3+} content dependence of lifetime at $^2F_{5/2}$ of Yb^{3+} by 466 nm excitation.

The decay time decreased at $x=0.1$ composition. It is considered that concentration quenching of Yb^{3+} occurred. The rise time should correspond to relaxation time from the $5d$ levels of Ce^{3+} to the $^2F_{7/2}$ of Yb^{3+}. However, the rise time was about 0.2 ms in all the samples and longer than lifetime ($\sim$100 ns) of Ce^{3+}:$5d$ level estimated from measurement of decay curve by 440 nm LD excitation. These results indicated that the energy transfer from the $5d$ level of Ce^{3+} to the $^2F_{5/2}$ of Yb^{3+} is not through direct process. It is considered that the longer rise time is due to slow nonradiative relaxation from a charge transfer state (CTS) to the $^2F_{5/2}$ level. In Yb^{3+}-doped YAG, the charge transfer absorption and the charge transfer luminescence have been reported.[20–23] In addition, it had been known that the emission of Ce^{3+} was quenched by the process of charge transfer state ($Ce^{4+}-Yb^{2+}$) in Ce^{3+}-doped crystal that consists of Yb, such as $LiYbF_4$,[24] $YbSiO_5$.[25,26] That is because the Ce^{3+} and Yb^{3+} changes to Ce^{4+} and Yb^{2+} easily. In a similar system, it was reported that Yb^{3+} IR emission in $Tb^{3+}-Yb^{3+}$ codoped Y_2O_3 by UV excitation was caused through $Tb^{4+}-Yb^{2+}$ charge transfer state.[12] Therefore, it is considered that the energy transfer from Ce^{3+} to Yb^{3+} may be caused through a CTS $Ce^{4+}-Yb^{2+}$ (Fig. 13).

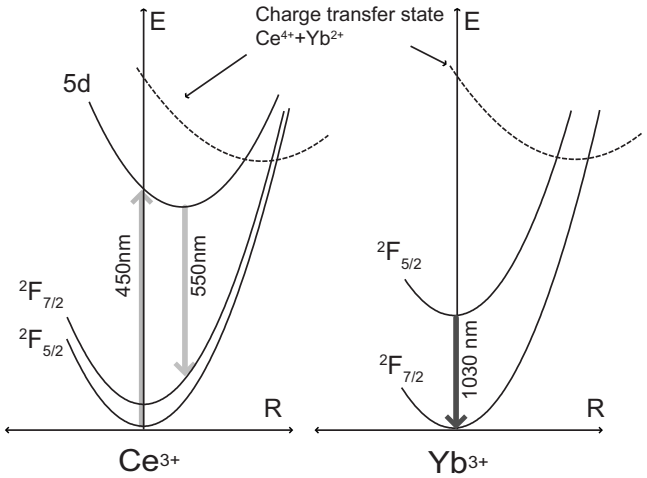

FIG. 13. Configuration coordinate model of emission and energy transfer from Ce^{3+} to Yb^{3+}. Dashed lines are $Ce^{4+}-Yb^{2+}$ charge transfer state.

VIII. CONCLUSION

The energy transfer from Ce^{3+} and sensitized luminescence of Yb^{3+} in polycrystalline YAG ceramics was observed. The quantum yields of Yb^{3+} emission upon Ce^{3+}:$5d$ level excitation were lower than that value expected for the ideal quantum cutting mechanism. In addition the relaxation time, which was estimated from measurement of Yb^{3+} decay curve by 440 nm LD excitation, from $5d$ levels of Ce^{3+} to $^2F_{7/2}$ of Yb^{3+} was not consistent to the lifetime of Ce^{3+} estimated from measurement of Ce^{3+} decay curve by 440 nm LD excitation. From the QY of Yb^{3+} emission by 935 nm excitation, the concentration quenching did not occur until $x=0.5$ Yb^{3+} concentration. Therefore, we indicated that the energy transfer from Ce^{3+} to Yb^{3+} in YAG was not direct process and has some nonradiative processes that were not the concentration quenching Yb^{3+}.

ACKNOWLEDGMENTS

These investigations were supported by the Toray Science Foundations and the Nippon Sheet Glass Foundation for Materials Science and Engineering.

[1] W. G. J. H. M. van Sark, A. Meijerink, R. E. I. Schropp, J. A. M. van Roosmalen, and E. H. Lysen, Sol. Energy Mater. Sol. Cells **87**, 395 (2005).
[2] W. Shockley and H. J. Queisser, J. Appl. Phys. **32**, 510 (1961).
[3] T. Trupke, M. A. Green, and P. Wurfel, J. Appl. Phys. **92**, 1668 (2002).
[4] D. L. Dexter, Phys. Rev. **108**, 630 (1957).
[5] W. W. Piper, J. A. DeLuca, and F. S. Ham, J. Lumin. **8**, 344 (1974).
[6] J. L. Sommerdijk, A. Bril, and A. W. de Jager, J. Lumin. **8**, 341 (1974).
[7] R. T. Wegh, H. Donker, A. Meijerink, R. J. Lamminmäki, and J. Hölsä, Phys. Rev. B **56**, 13841 (1997).
[8] R. T. Wegh, H. Donker, K. D. Oskam, and A. Meijerink, Science **283**, 663 (1999).
[9] R. T. Wegh, E. V. D. Van Loef, and A. Meijerink, J. Lumin. **90**, 111 (2000).
[10] W. Stręk, A. Bednarkiewicz, and P. J. Dereń, J. Lumin. **92**, 229 (2001).
[11] P. Vergeer, T. J. H. Vlugt, M. H. F. Kox, M. I. den Hertog, J. P. J. M. van der Herden, and A. Meijerink, Phys. Rev. B **71**, 014119 (2005).
[12] S. Ye, B. Zhu, J. Chen, J. Luo, and J. R. Qiu, Appl. Phys. Lett. **92**, 141112 (2008).
[13] J. L. Yuan, X. Y. Zeng, J. T. Zhao, Z. J. Zhang, H. H. Chen, and X. X. Yang, J. Phys. D: Appl. Phys. **41**, 105406 (2008).
[14] Q. Y. Zhang, G. F. Yang, and Z. H. Jiang, Appl. Phys. Lett. **91**, 051903 (2007).
[15] X. Liu, Y. Qiao, G. Dong, S. Ye, B. Zhu, G. Lakshminarayana, D. Chen, and J. Qiu, Opt. Lett. **33**, 2858 (2008).
[16] Y. Narukawa, I. Niki, K. Izuno, M. Yamada, Y. Murazaki, and T. Mukai, Jpn. J. Appl. Phys., Part 2 **41** L371 (2002).
[17] S. Fujita, A. Sakamoto, and S. Tanabe, IEEE J. Sel. Top. Quantum Electron. **14**, 1387 (2008).
[18] JCPDS PDF No. 33-0040.
[19] JCPDS PDF No. 23-1476.
[20] L. van Pieterson, M. Heeroma, E. de Heer, and A. Meijerink, J. Lumin. **91**, 177 (2000).
[21] N. Guerassimova, N. Garnier, C. Dujardin, A. G. Petrosyan, and C. Pedrini, Chem. Phys. Lett. **339**, 197 (2001).
[22] M. Nikl, A. Yoshikawa, and T. Fukuda, Opt. Mater. (Amsterdam, Neth.) **26**, 545 (2004).
[23] I. Kamenskikh, C. Dujardin, N. Garnier, N. Guerassimova, G. Ledoux, V. Mikhailin, C. Pedrini, A. Petrosyan, and A. Vasil'ev, J. Phys.: Condens. Matter **17**, 5587 (2005).
[24] J. W. M. Verweij, C. Pédrini, D. Bouttet, C. Dujardin, H. Lautesse, and B. Moine, Opt. Mater. (Amsterdam, Neth.) **4**, 575 (1995).
[25] D. W. Cooke, R. E. Muenchausen, B. L. Bennett, K. J. McClellan, and A. M. Portis, J. Lumin. **79**, 185 (1998).
[26] J. F. Rivas-Silva, S. Durand-Niconoff, T. M. Schmidt, and M. Berrondo, Int. J. Quantum Chem. **79**, 198 (2000).